A multiparameter investigation of syngas/diesel dual-fuel engine performance and emissions with various syngas compositions

R. Rabello de Castro, Pierre Brequigny, Christine Mounaïm-Rousselle

A multiparameter investigation of Syngas/diesel Dual-Fuel Engine performance and emissions with various syngas compositions

R. Rabello de Castro, P. Brequigny*, C. Mounaïm-Rousselle

Université d'Orléans, INSA-CVL, PRISME, EA 4229, F45072 Orléans, France

*** corresponding author : pierre.brequigny@univ-orleans.fr**

Abstract

Syngas, also known as producer gas or wood gas, is a gaseous biofuel produced by gasification of biomass. It is mainly composed of hydrogen and carbon monoxide with a smaller share of methane, all diluted by nitrogen and carbon dioxide. Despite having carbon in its composition, since it is made from biomass, it is considered low to zero-carbon and being so makes it one candidate for reducing carbon emissions of internal combustion engines. This work focuses on the effect of different syngas compositions on the performance and the exhaust emissions of compression ignition engine with decane pilot injection as a diesel surrogate. Results showed that thermal efficiencies over 39% are possible with a variety of syngas with less than 10% energy contribution of decane. NO_x and soot emissions were generally lowered by increasing the syngas/decane ratio, whereas CO and Total HC emissions increased. Additionally, relations between engine performance/emissions and fundamental properties of varying Syngas compositions were established. Further investigation on other combustion properties, such as stretch sensitivity of the syngas/air flame, are needed in order to better predict optimum operability.

Keywords: Syngas-fueled compression engine, diesel pilot injection, Dual-Fuel, syngas compositions, Performances, Emissions

1 Introduction

A considerable amount of pressure has been put on the energy sector to shift towards clean and renewable energy. In fact, to achieve the goal set by more than 100 countries of net-zero carbon emissions by 2050, all sectors of the economy will have to endure significant change[1]. While it might appear to most that, the only solution to achieve this goal, is a complete transition to a combustion-free energy sector, this might not be simple to accomplish.

Given the context presented above the use of biofuels presents itself as an alternative that would reduce global CO_2 emissions with more affordable costs and simpler technologies. Syngas, also known as producer gas and wood gas, is a general classification given to flammable mixtures produced by the gasification of biomass. Gasification is a process that converts the molecules in the biomass (such as cellulose) to CO, H_2 and CO_2. It should not be confused with biogas where the biomass is transformed mainly into CH_4 and CO_2 through fermentation. As a waste-to-energy process, gasification competes with landfilling and methanation, but the carbon footprint of the syngas scenario is higher than landfilling [2] and can be in some case better than the biogas scenario [3]. The challenge when fueling an internal combustion engine (ICE) with syngas is the inherent variability in composition that is a result of several factors such as the biomass origin [4] and the gasification process [5]. Typical values for H_2, CO and CH_4 contents stay between 10-20%, 13-24% and 0-7% in volume respectively[5,6]. Moreover, regarding dilution, air-fed gasifiers typically produce syngas that contains from 45 to 60% N_2 content and 10-20% CO_2. If oxygen or steam gasification is used, N_2 content can be close to zero but these methods tend to be more expensive[6].

Nomenclature

SI	Spark Ignition	$\dot{V}$	Volumetric Flowrate
CI	Compression Ignition	$\dot{m}$	Mass Flowrate
HRR	Heat Release Rate	h	Heat Transfer Coefficient
η	Efficiency	LHV	Lower Heating Value
SOI	Start of Injection	P	Pressure
b	Cylinder Bore	T	Temperature
V_{cyl}	Diplaced Volume	ν	Piston linear speed
CAD	Crank Angle Degree	CAXX	CAD where XX % of the fuel is burned
IMEP	Indicated Mean Effective Pressure	$IMEP_{cov}$	Coefficient of IMEP variation
ATDC	After Top Dead Center	BTDC	Before Top Dead Center
MPRR	Maximum Pressure Rise Rate	LFS	Laminar Flame Speed
RPM	Revolutions Per Minute	THC	Total Hydrocarbons

Syngas can be used as fuel in ICE both in Spark Ignition (SI) [7,8] and Compression Ignition (CI) Engine [9–14]. Studies in SI engine are mainly focused on the auto-ignition propensity of the syngas. Sridhar et al. [7] showed that, due to the auto-ignition resistivity of syngas, it was possible to increase the compression ratio of SI engine with minimum knock risk thus improving the efficiency. Arunachalam and Olsen [8] studied the knock propensity as a function of different syngas compositions. Their work is noticeable since it compares "real" compositions containing all the main components of the syngas namely H_2, CO, CH_4, CO_2 and N_2. Regarding CI engines, Guo et al.[9] have investigated the effects of syngas energy fraction, the reactive fuel injection timing and the load on emissions and efficiency for two distinct simulated syngas compositions from air-fed gasifiers (48% N_2 and 13% CO_2 concentrations) and one oxygen-fed gasifier composition (6% N_2 only) in dual-fuel mode. The

effects of syngas substitution were a reduction in soot and NO_x emissions but higher CO emissions for the two compositions with the highest N_2 content in syngas. Between these two high-dilution compositions, the one with more CO and less H_2 produces more CO at the exhaust and lower overall efficiencies. Some other studies used real syngas directly from a gasifier. Rinaldini et al.[10] managed a maximum real syngas energy fraction of 60% at 50 N.m and 27% at 300 N.m of torque. Sharma and Kaushal[15] also tested real syngas from a downdraft gasifier on a variable compression ratio CI engine. The result of increasing the compression ratio from 12:1 to 18:1 was a reduction of CO and THC emissions with a simultaneous increase in efficiency. Roy et al.[16] tested the effects of injection timing and equivalence ratio on performance and emissions as a function of H_2 content in Syngas. Diesel substitution levels of over 96 % under low or high H_2 content were achieved at an Indicated Mean Effective Pressures (IMEP) of 14 bars but the highest H_2 content composition resulted in a higher thermal efficiency. However, this also led to an increase in NO_x emissions.

The use of Syngas in a CI engine in dual-fuel mode has the advantage to have a flex-fuel energy system, especially for off-grid stationary application. In dual-fuel mode, due to the pilot injection of reactive fuel (as diesel fuel), there is the added complexity of the poorly understood physicochemical interactions of the gaseous syngas combustion interactions with the liquid pilot fuel spray. Currently, natural gas or methane dual-fuel operation are well covered by the literature [17–21] but syngas less. Moreover, to correctly optimize dual-fuel syngas CI engines, the effects of its composition should be well understood. The challenge, addressed in the present paper, when studying the influence of syngas composition on dual-fuel engine performance is not fed the engine with real syngas but to control the compositions that are representative of what is possible to produce from gasification, as an input parameter and, in parallel, identifying the impact of each gas component on performance and emission parameters. The novel approach chosen for this study is to consider three compositions that

represent the typical production of three gasifier types: Fluidized Bed, Fixed-bed Updraft and Fixed-bed Downdraft (respectively indicated as Fluidbed, Updraft and Downdraft in following), detailed in Table 1, and originally defined by Bridgwater[5] as well as to keep a maximum syngas energy fraction(>60%). Indeed, the previous studies introduced above are mainly conducted with a unique syngas composition or are numerical studies [12–14,22]. As a new insight of syngas use in dual-fuel mode, the effect of syngas composition will be studied as well as the contribution of each component of the syngas experimentally on an engine test bench. It should be noted that the maximum laminar flame values for 3 Syngas compositions displayed in Table 1 have been determined previously[23–25].

Table 1: Syngas Compositions.

	H_2 (%Vol)	CO (%Vol)	CO_2 (%Vol)	CH_4 (%Vol)	N_2 (%Vol)	Stoichiometric Air/ Fuel ratio (mol/mol) (*mass/mass*)	LHV (MJ/m³ of gas)	Maximum laminar flame speed at 298K and 1bar (cm/s)
Fluidbed	9	14	20	7	50	1.21 *(1.25)*	4.2	15.4
Updraft	11	24	9	3	53	1.12 *(1.24)*	4.4	30.7
Downdraft	17	21	13	1	48	1.00 *(1.13)*	4.8	36.7

The global objective of this study is to identify what are the fundamental combustion and physical properties of syngas that determine engine performance and operating limits in dual-fuel mode. For that, the effects of the pilot fuel quantity and equivalence ratio of premixed syngas/air on engine performance and emissions are analyzed for each composition. Moreover, to highlight the contribution of CH_4 and CO_2 contents, an additional analysis is carried out with ternary mixtures of H_2/CO/N_2.

2 Experimental Method

In this section the engine characteristics, experimental method and the post-processing method are described.

2.1 Experimental Setup

The experimental setup consists of a research PSA DW10 based engine test bench converted to single-cylinder operation with 3 cylinders not fueled. The engine speed, driven by an electric motor, is maintained at 1200 RPM. The engine speed for genset application is usually 1500 RPM. Unfortunately, it was not possible with our setup due to important vibrations of the intake/exhaust pipes and bench. The engine characteristics are described in Table 2.

Table 2: Engine Characteristics.

Displaced Volume	499 cm^3
Bore	85 mm
Stroke	88 mm
Rod length	145 mm
Compression Ratio	17:1
Piston Bowl Type	"Mexican hat"
Firing TDC position	0 CAD
Intake Valve Opening	351 CAD ATDC
Intake Valve Closure	157 CAD BTDC
Exhaust Valve Opening	140 CAD ATDC
Exhaust Valve Closure	366 CAD ATDC
Oil and Coolant Temperature	85 °C
Max Brake Power (for the commercial multi-cylinder engine)	120 kW @ 3750 rpm
Max Torque (for the commercial multi-cylinder engine)	340 N.m @ 2000 rpm

In order to obtain the desired intake charge compositions a series of mass flow meters, as specified in Table 3, are used. The resulting uncertainty for the premixed syngas/air equivalence ratio, $\phi_{premixed}$ (eq. 1) of the intake charge is ±2%. The mixing of the syngas/air charge is ensured by the intake plenum (visible in Fig. 1) which also enables to damper pressure oscillations at the intake port.

Table 3: Mass Flow Controllers.

Gas Type	Flowmeter / Controller	Full Scale	Uncertainty
Air	Emerson F025S	1100 NL/min	±0.5%
N_2	Brooks 5851S	100 NL/min	±0.9%
CO	Brooks 5851S	100 NL/min	±0.9%
H_2	SLA5850	50 NL/min	±1,0 %
CO_2	SLA5850	37 NL/min	±1.0%
CH_4	SLA5850	5 NL/min	±1.0%

The pilot injection is discharged by a Bosch CRI 2.2 six-holes common-rail injector operating at a reduced pressure of 200 bar to guarantee minimal injection quantities with sufficient injection duration. The injector was previously characterized by means of an IAV type-K flow rate analyzer to provide the injection rate profiles and injection quantities as a function of the injection duration. Decane ($C_{10}H_{22}$) was used as a surrogate for diesel fuel to facilitate future CFD simulations and kinetics one with Madison kinetic mechanism of Ren at al.[26] to determine fundamental combustion properties of syngas/decane/air mixtures.

The gaseous equivalence ratio, $\Phi_{premixed}$, is calculated as the O_2 volumetric flowrate required for stoichiometry divided by the real O_2 volumetric flowrate (Eq. 1). A global equivalence ratio (ϕ_{global}) can be also calculated as a function of the pilot fuel amount and the stoichiometric mass air/fuel ratio of decane (15.03) as indicated in Eq. 2.

$$\phi_{premixed} = \frac{0.5\dot{V}_{CO} + 0.5\dot{V}_{H_2} + 2.0\dot{V}_{CH_4}}{0.21\dot{V}_{Air}} \#(1)$$

$$\phi_{global} = \phi_{premixed} + \frac{15.03}{\dot{m}_{air}/\dot{m}_{pilot}} \#(2)$$

Additionally, the energy share of the pilot fuel (decane) energy of the total supplied energy is defined as follows:

$$E_{pilot} = 100 \cdot \frac{\dot{m_{inJ}} LHV_{C_{10}H_{22}}}{\dot{m_{inJ}} LHV_{C_{10}H_{22}} + \dot{m}_{syngas} LHV_{syngas}} \quad \#(3)$$

A MEXA 7100D-EGR HORIBA gas analyzer is capable of measuring O_2 (magneto-pneumatic detector), CO and CO_2, (non-dispersive infrared absorption analyzer), NO_x (chemiluminescence analyzer) and total unburnt Hydrocarbons (THC) (flame ion analyzer) concentrations with a precision of 1 ppm for all gases. These concentrations are converted to specific emissions. Additionally, an AVL 415S smoke-meter, with a detection limit of 0.02 mg/m³ is used to provide soot emission data. The full experimental setup is schematized in **Erreur ! Source du renvoi introuvable.**.

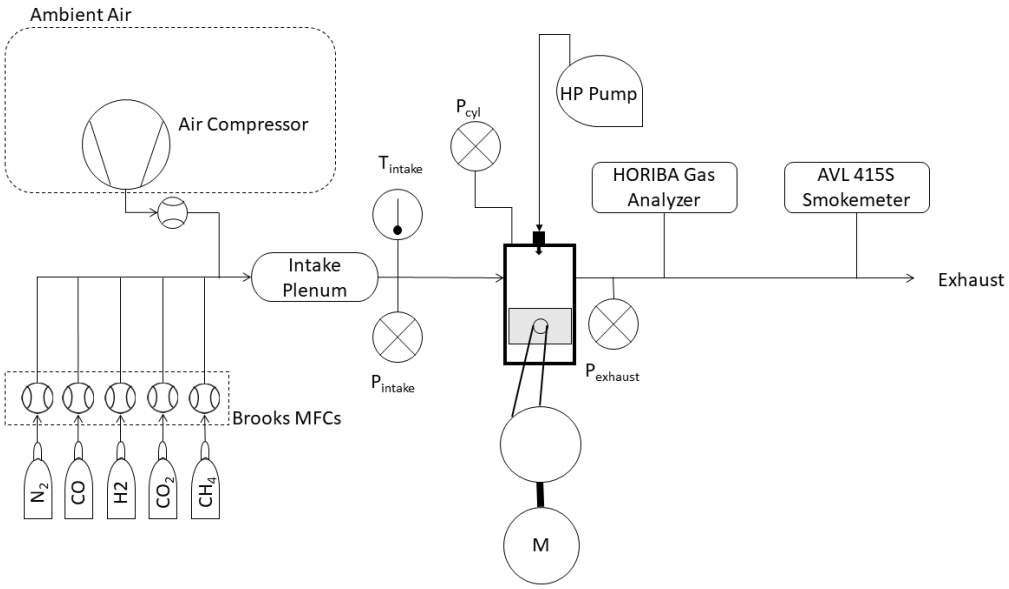

Figure 1: Experimental Setup scheme.

2.2 Post-processing method

From the averaged in-cylinder pressure, calculated over 100 consecutive cycles that are measured by a Kistler 6043A piezo-electric pressure transducer (accuracy of ± 2.0 %), the gross Heat Release Rate (HRR) is estimated with the following equations:

$$\boldsymbol{HRR\ (J/CAD)} = \frac{\boldsymbol{\gamma}}{\boldsymbol{\gamma - 1}}\boldsymbol{PdV} + \frac{\boldsymbol{1}}{\boldsymbol{\gamma - 1}}\boldsymbol{VdP} + \boldsymbol{dQ_{wall}} \#(\mathbf{4})$$

$$dQ_{wall}(J/CAD) = h.S.(T - T_{wall}) \#(5)$$

$$h\ (J.K^{-1}.m^{-2}) = 3.26b^{-0.2}P^{0.8}T^{-0.55}v^{0.8} \#(6)$$

The heat transfer coefficient *h* is determined using the correlation proposed by Woschni [27]. The integrated value of $dQ_{combustion}$ is used to determine the mass of fuel burnt (MFB). Cylinder wall temperature, T_{wall}, is estimated at 423 K. The calculation is first done with a constant heat capacity ratio, γ, to obtain a first MFB. Then γ is reassessed from the MFB with the mole fractions of all six components (N_2, O_2, CO, H_2, CO_2, CH_4) for the unburnt gases and with the emissions data for the burnt gases using NASA polynomials equation. Equations 4-6 are then recalculated with this variable γ and the definitive MFB value is obtained.

The thermal efficiency is calculated with the following equation:

$$\eta_{thermal} = \frac{IMEP * V_{cyl} * \dot{m}_{total}}{LHV_{CO}.\dot{m}_{CO} + LHV_{H_2}.\dot{m}_{H_2} + LHV_{CH_4}.\dot{m}_{CH_4} + LHV_{C_{10}H_{22}}.\dot{m}_{C_{10}H_{22}}} \#(7)$$

The combustion efficiency is calculated by doing the oxygen balance between intake and exhaust related to the total equivalence ratio:

$$\eta_{combustion} = \frac{0.21\dot{m}_{air-intake} - \dot{m}_{O_2-exhaust}}{\dot{m}_{O_2-theoretically\ burning}} \#(8)$$

3 Results and discussion

3.1 Effect of premixed equivalence ratio

To study the effect of syngas/air equivalence ratio, the injection duration was kept constant at 500 μs (i.e. 0.61 mg) with an increase of syngas amount in the intake charge. The start of injection (SOI) was optimized to guarantee maximum IMEP. Premixed equivalence ratio $\phi_{premixed}$ was varied to 0.3, 0.5, 0.7 and 1.0 for all three compositions except for Fluidbed for which $\phi_{premixed} = 1.0$ induced very unstable combustion, i.e. $IMEP_{cov}$ >10%. In this

section, increasing $\phi_{premixed}$ leads to a syngas mass flowrate increase but an air mass flowrate decrease in order to keep a constant intake pressure (i.e. 1 bar).

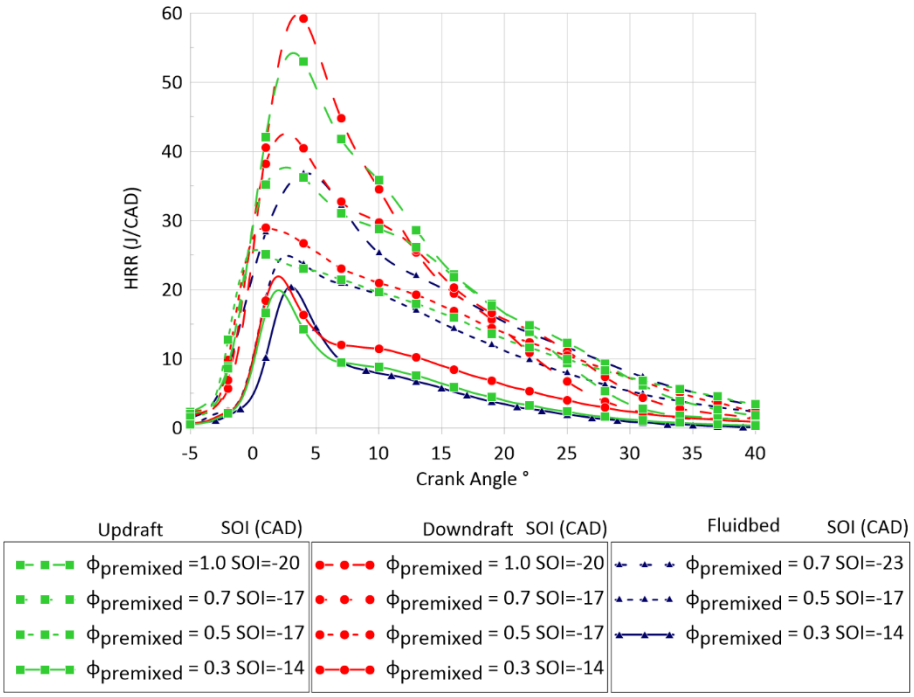

Figure 2: Evolution of Heat Release Rate for all premixed equivalence ratios and the three compositions (1200 RPM, P_{intake} = 1 bar, T_{intake}= 300K).

In Figure 2 the HRR traces show that, for all compositions, the increase of $\phi_{premixed}$ induces a transition from a two-phase to a single-phase combustion evolution. This could be linked to a reduction in the ignition delay of the syngas/air mixtures with $\phi_{premxed}$ so, in practice, instead of having the first auto-ignition of the decane charge followed by a slow flame of syngas/air mixture, both fuels start burning simultaneously. When the pilot injection occurs, i.e 20 CAD BTDC, the liquid fuel is atomized and has enough time to mix with the nearest surrounding syngas/air premixed mixture. Therefore, the ignition of the liquid pilot spray will also ignite the surrounding premixed charge of syngas especially if the syngas is in sufficient quantity as for the stoichiometric syngas/air case. When $\phi_{premixed}$ is lower, the decane is introduced later, so less mixing with syngas/air, and less syngas is available. Therefore, the

179 decane will first ignite before the ignition of the premixed syngas charge. It should also be
180 noted that the maximum HRR increases with $\phi_{premixed}$ but the delay does not seem to be
181 affected after $\phi_{premixed} \geq 0.5$ for downdraft and updraft. Higher H_2 concentrations in the
182 syngas composition induce higher peak of HRR. This is consistent with the findings of Dhole
183 et al.[28] and Roy et al.[16]. For same equivalence ratio, the overall shape of the profiles is
184 not affected by the Syngas composition as also highlighted by the In-Cylinder Pressure in
185 Figure 3. The In-Cylinder Pressure shows that the $\phi_{premixed}$ increase leads to a higher peak
186 pressure and a longer combustion tail for downdraft. The major change is when increasing
187 from 0.3 to 0.5 after that the pressure traces show similar envelope. For the composition
188 effect, Updraft and Downdraft present the same pressure trace while the peak pressure is a bit
189 lower for Fluidbed as expected due to its lower energy content. The differences, between both
190 compositions, in terms of start of combustion are highlighted in Figure 3b (in-cylinder
191 pressure traces of Updraft and Fluidbed are available as supplementary materials). It can also
192 be noted from Figures 3 that SOI remains between -14 and -20 CAD for Updraft and
193 Downdraft and that the range is a bit wider for Fluidbed, i.e. down to -23 CAD. Moreover, in
194 order to get maximum IMEP with minimum $IMEP_{cov}$, the SOI is advanced with the increase
195 of $\phi_{premixed}$.

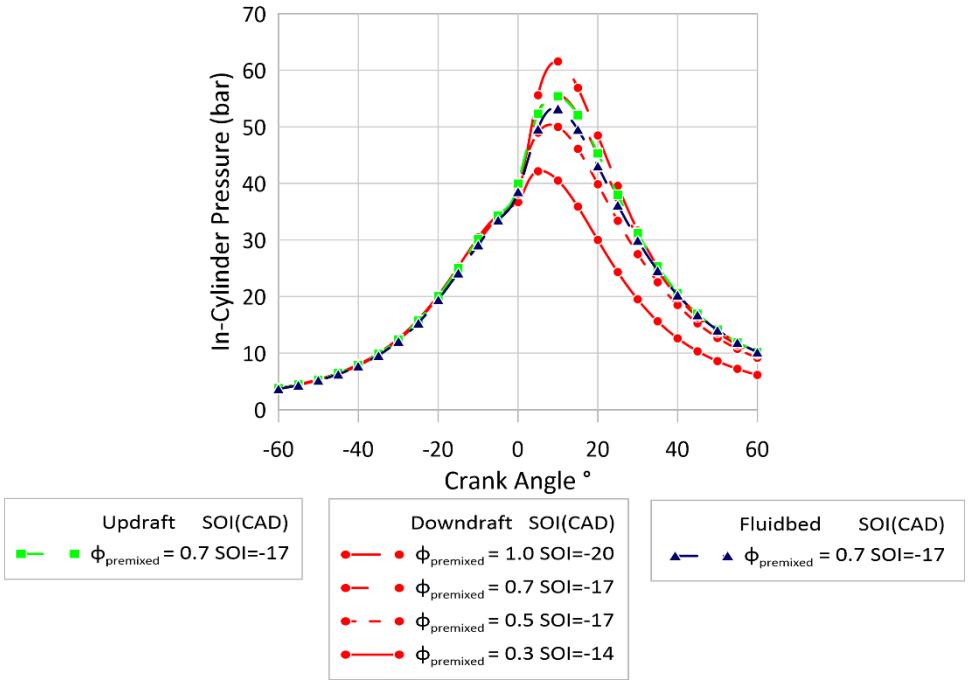

196

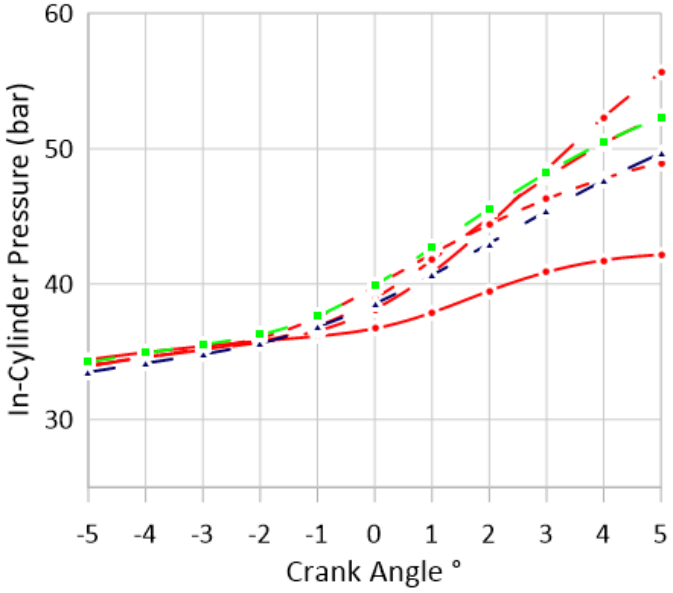

197

198 **Figure 3. (a) Evolution of In-Cylinder Pressure for all premixed equivalence ratio for**

199 **Downdraft and only at $\phi_{premixed} = 0.7$ for Updraft and Fluidbed, (b) zoomed between**

200 **-5 and 5 CAD. (1200 RPM, Pintake = 1 bar, Tintake= 300K)**

201 Figure 4a displays the corresponding IMEP and energy share of the pilot E_{pilot}. First, in

202 agreement with HRR and in-cylinder pressure traces, IMEP increases with $\phi_{premixed}$ since

203 more energy is introduced. Then it is worth noticing that, in all cases, the energy share of the

pilot stays below 21% of the total energy amount. Since the injected quantity of decane is maintained constant, the pilot energy share decreases with $\phi_{premixed}$. Figure 4b shows the $IMEP_{cov}$ as well as the MPRR as a function of $\phi_{premixed}$. It can be seen that for premixed equivalence ratio greater than 0.5, the combustion is quite stable for all compositions, i.e. IMEPcov below 6%, except for Fluidbed (8% for IMEPcov). For $\phi_{premixed} = 0.3$, the combustion is more likely to be unstable (up to 13% of IMEPcov for Downdraft) but it remains possible to operate the engine. Regarding combustion noise, the maximum pressure rise rate (MPRR) increases with $\phi_{premixed}$ because of energy input increase and H_2 content in the syngas composition. The syngas compositions can be ranked, Fluidbed, Updraft, Downdraft from lower to higher maximum pressure gradient. For Downdraft and Updraft at stoichiometric premixed equivalence ratio, it should be mentioned that the MPRR is at the limit of excessive combustion noise (4 bar/CAD) [29].

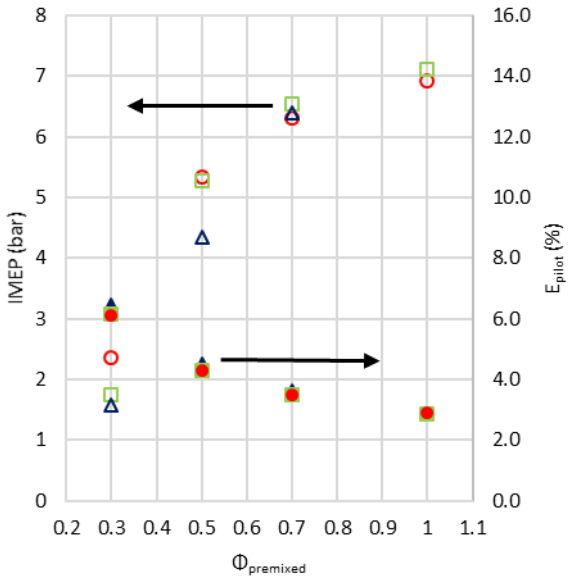

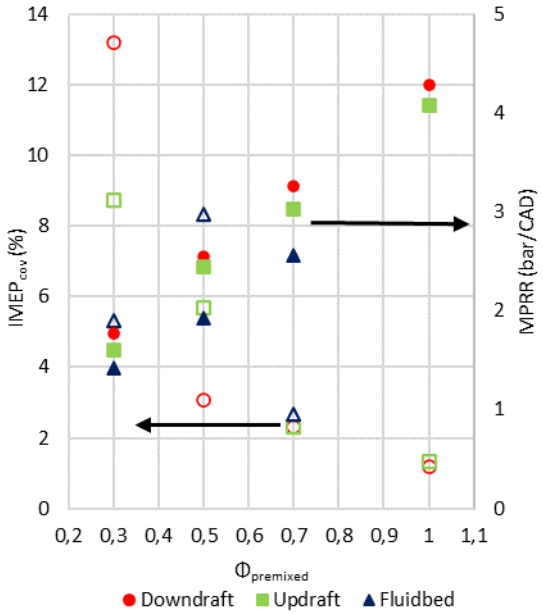

Figure 4. a) IMEP (empty symbols) and Epilot (filled symbols) and b)IMEPcov (empty symbols) and MPRR (filled symbols) as function of $\phi_{premixed}$

In Figure 5, both the ignition delays from the pilot injection timing and the first part of the combustion development are plotted as a function of the equivalence ratio. First, it can be noted that the increase in premixed equivalence ratio also increases the ignition delay. It is probably explained by the fact that the start of injection (SOI) is advanced with the increase in premixed equivalence ratio. Indeed, it should be reminded that SOI is advanced in order to keep a maximum IMEP and therefore a relatively constant CA50. This is especially verified for the Fluidbed composition, for which the increase is more linear and stronger than for the Downdraft and Updraft ones. This is probably explained by the higher CO_2 content (20%) of Fluidbed composition that contributes to delay the autoignition. Yet, the duration of the first half of the combustion, represented by CA50-CA10, strongly decreases from $\phi_{premixed} = 0.5$ onwards. This is due to the increased reactivity of the premixed charge and the increase of the flame propagation speed.

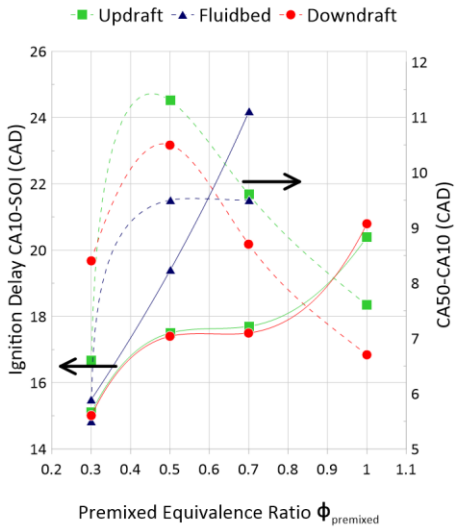

232

233 **Figure 5: Effect of premixed equivalence ratio on ignition phasing (continuous lines) and**

234 **first half of combustion (dotted lines) (1200 RPM P_{intake} = 1 bar T_{intake}= 300K).**

235 Figure 6 presents the thermal and combustion efficiencies and emissions as a function of

236 premixed equivalence ratio for the three Syngas compositions. Both combustion and thermal

237 efficiencies are bell-shaped reaching peak values around 98% and 39% respectively for

238 Downdraft and Updraft compositions. For Fluidbed, efficiencies continuously increase but the

239 curves start to bend. Since premixed stoichiometric equivalence ratio was not achievable, it is

240 not possible to forecast for which equivalence ratio efficiencies will start to decrease. The

241 lowest combustion efficiency, reached for the ultra-lean premixed charge, induces, as

242 expected, the highest CO and THC emissions. The minimum CO and THC emissions are

243 obtained when $\phi_{premixed}$ is between 0.5 – 0.7 and as expected where efficiencies are the

244 highest ones. Overall, this effect of the premixed equivalence ratio on the CO and THC

245 emissions confirms the ones observed by Roy et al.[16]. For NO_x emissions, also the lowest

246 values are obtained at $\phi_{premixed} = 0.5$, with the highest ones reached at the stoichiometric

247 syngas/air mixture. This evolution is not expected as the NOx emission peak is reached in

248 lean side in classical SI engine. It is indeed surprising to observe that minimum NOx

249 coincides with minimum CO, but since syngas is a highly diluted fuel (about 50% N_2, 10 to

20 %CO_2), its combustion temperature is very low leading to low NOx levels even in lean mixtures where CO emission is also minimum. Similar trends were observed numerically for NOx emission but not for CO one (Kousheshi et al. [30]). For all operating conditions, soot emissions were below the detection limit of the measurement device.

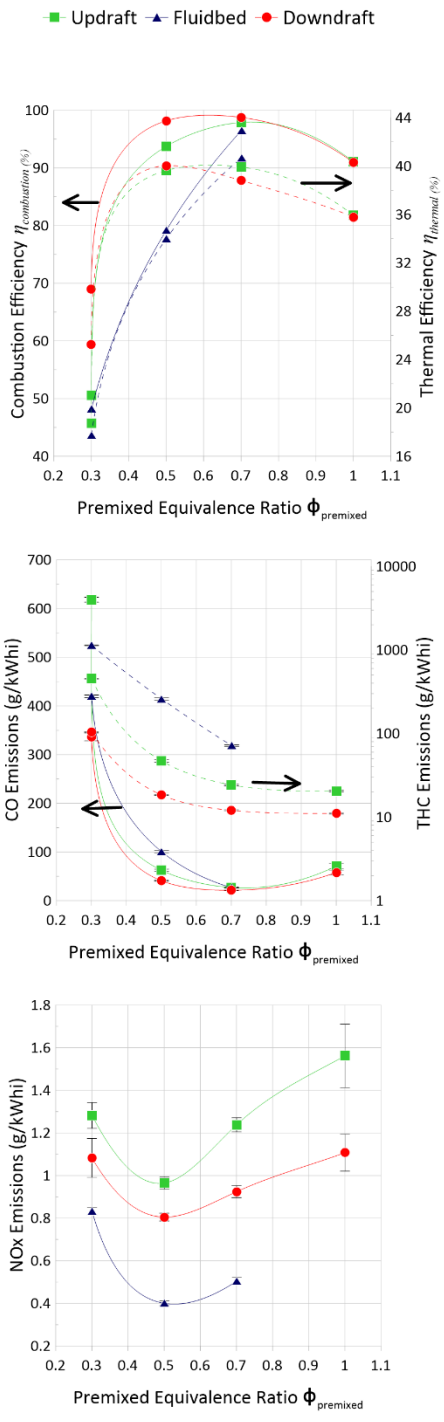

Figure 6: Efficiencies and exhaust gases emissions as a function of premixed equivalence ratio for the three Syngas compositions (1200 RPM, P_{intake} = 1 bar, T_{intake}= 300K, Optimum SOI).

3.2 Effect of pilot fuel injection quantity

In the previous section, since the optimal premixed equivalence ratio was found to be around $\phi_{premixed} = 0.7$, the effect of the pilot injection was evaluated at this particular value, while the injection duration was varied from 250 μs to 1000 μs, i.e. corresponding to 0.11 to 4.86 mg of decane injected per cycle (see Table 4). First, to evaluate the contribution of the pilot amount in the combustion development, the pilot fuel is first injected in air (without syngas) and then in air plus 5%$_{vol}$ CO_2 and 20%$_{vol}$ N_2 concentrations (equivalent charge dilution as the downdraft case).

Table 4: Experimental conditions to study the effect of pilot fuel injection quantity.

Case	Injection Duration (μs)	Decane injected mass (mg)	ϕ_{global}	Pilot fuel energy share (%)	IMEP (bar)	SOI (CAD) ATDC
Downdraft/Air	250	0.11	0.71	0.6	5.7	-17
	500	0.61	0.74	3.3	6.3	
	750	2.16	0.83	10.9	6.8	
	1000	4.86	1.0	21.7	7.4	
Air	500	0.61	0.02	100	0.4	-11
	750	2.16	0.08		1.2	
	1000	4.86	0.17		2.8	
Air/Diluents	750	2.16	0.1		0.7	-16
	1000	4.86	0.22		2.0	

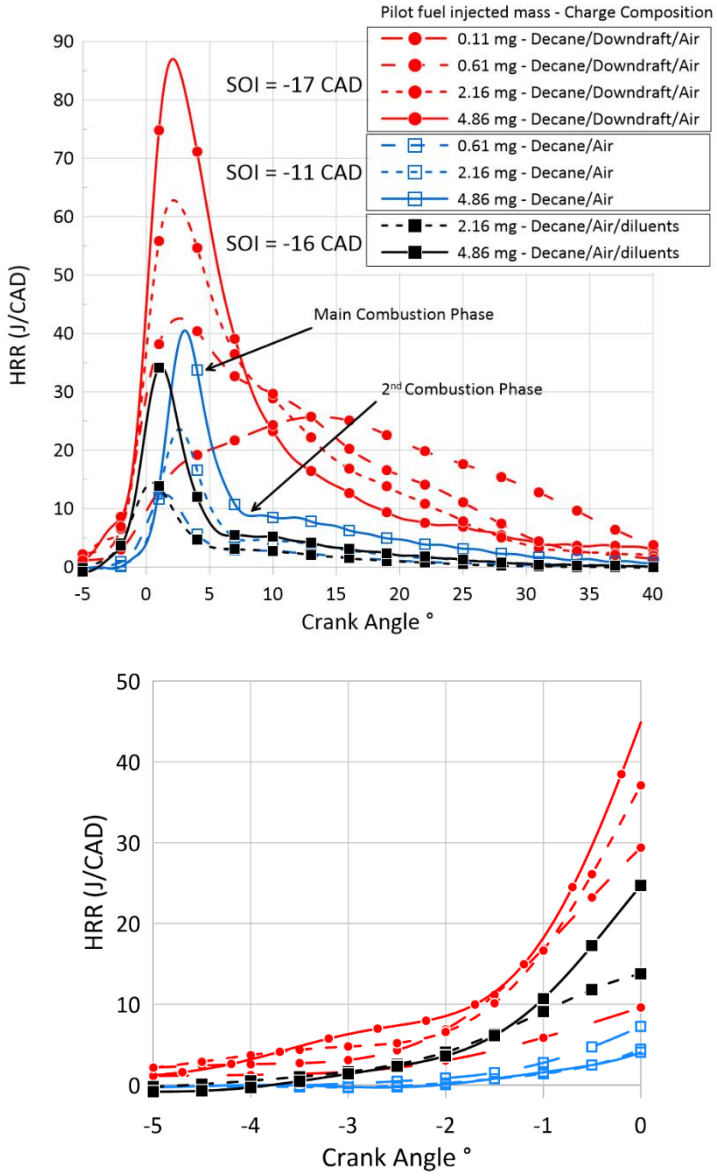

Figure 7(a): Heat release rate from the fuel pilot injection in air and air with diluents compared to downdraft dual-fuel. ($\phi_{premixed} = 0.7$) and (b)zoom between -5 and 0 CAD

In Figure 7, it can be clearly seen that the ignition delay of the reactive fuel, decane from pilot injection, is similar in air with diluents as with the presence of syngas. However, it can be noted that for the highest quantity of liquid pilot injection, i.e. 4.86 mg, an earlier heat release can be observed between -5 and -2 CAD before TDC, smaller than the major rise in HRR that follows – when decane is injected in premixed syngas/air. This low-temperature heat release

could indicate a two-stage ignition process that does not occur when the decane injection is done in non-reactive medium (i.e. air or air/diluent). In these cases, the combustion occurs in two phases: the main combustion phase due to the premixing of decane with air and a second one, slower due to the diffusion-controlled combustion. The distinction between the phases is less clear when syngas is premixed with the intake charge but there is still an inflexion point after the peak in HRR for 0.61 and 2.16 mg quantity injected at around 7 and 9 CAD ATDC respectively.

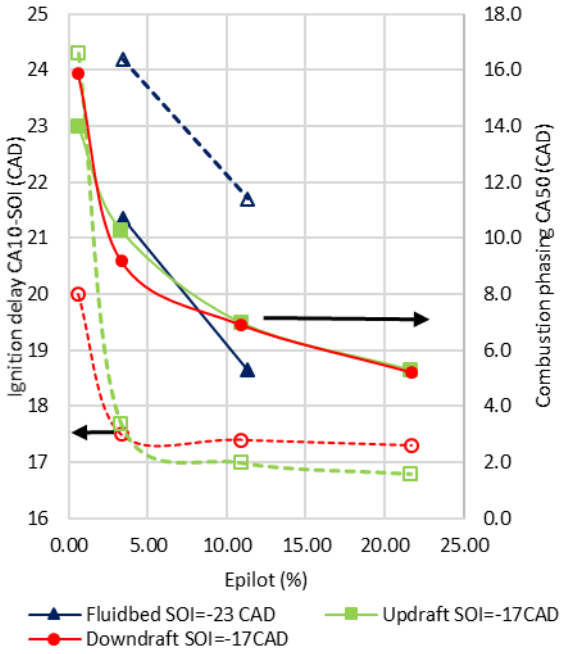

Figure 8: Effect of pilot fuel energy share on ignition delay (empty symbols, dashed lines) and combustion phasing CA50 (filled symbols, continuous lines) for three Syngas compositions (1200 RPM, P_{intake} = 1 bar, T_{intake}= 300K , $\phi_{premixed} = 0.7$).

In Figure 8, the effect of decane addition on the ignition timing and the combustion phasing (CA50) is presented for the 3 syngas compositions. For the Fluidbed composition, stable combustion could not be achieved at the lowest and highest pilot fuel injection durations therefore only two data points are presented. This behavior can be attributed to the high CO_2 concentrations of Fluidbed combined with the comparatively low H_2 and CO contents. For

updraft and downdraft ones, the ignition delay seems to stabilize once enough decane is injected (over 10% of the total available energy). But, the combustion phasing is monotically advanced with the addition of decane, as expected from the HRR profiles presented in Figure 7 for the Downdraft composition. Basically, increasing the energy share from the more reactive fuel will reduce the ignition delay of the whole fuel charge as observed on CA10-SOI, the decane being easier to auto-ignite. This will lead to a shift of the CA50 and globally of the whole combustion earlier in the cycle. For Downdraft, $IMEP_{cov}$ decreases from 2.4 down to 1.08 % and MPRR increases from 1.2 up to 6.9 bar/CAD as E_{pilot} increase. For Updraft, the trends and values are very similar to Downdraft. However, for Fluidbed, $IMEP_{cov}$ decreases from 2.6 down to 2 % and maximum pressure gradient increases from 2.6 up to 4.8 bar/CAD with E_{pilot} increases. Hence, and as expected, ranking in terms of combustion stability and noise is the same as the one observed in the previous section.

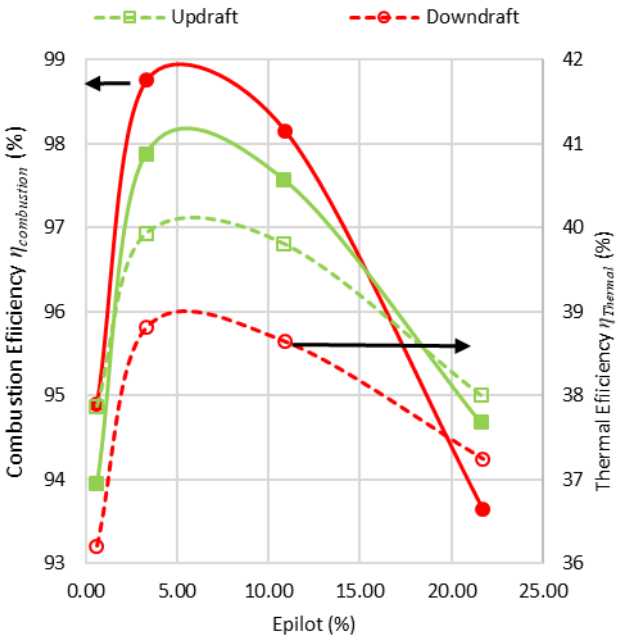
Updraft
Downdraft
Combustion Efficiency $\eta_{combustion}$ (%)
Thermal Efficiency $\eta_{Thermal}$ (%)
Epilot (%)
99
98
97
96
95
94
93
42
41
40
39
38
37
36
0.00
5.00
10.00
15.00
20.00
25.00

307

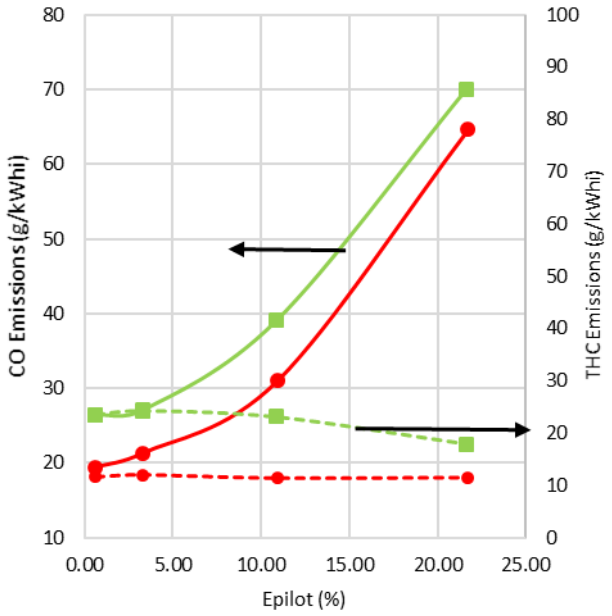
CO Emissions (g/kWhi)
THC Emissions (g/kWhi)
Epilot (%)
80
70
60
50
40
30
20
10
100
90
80
70
60
50
40
30
20
10
0
0.00
5.00
10.00
15.00
20.00
25.00

308

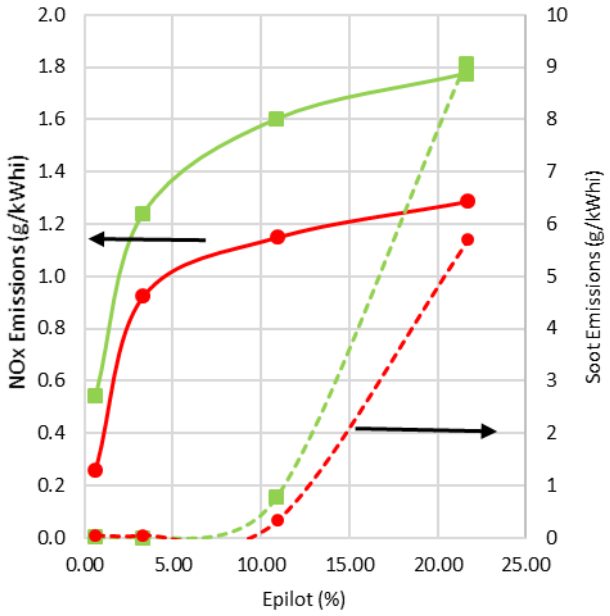

Figure 9: Efficiencies and emissions as a function of decane energy share for the three Syngas compositions. Filled symbols/continuous lines : Combustion efficiency, CO and NOx emissions for a,b and c respectively. Empty symbols/Dashed lines: Thermal Efficiency, THC and Soot emissions for a, b and c respectively

(1200 RPM, $P_{intake} = 1$ bar, $T_{intake} = 300$K, $\phi_{premixed} = 0.7$).

In Figure 9, for Updraft and Downdraft compositions, the combustion and thermal efficiencies are bell shaped with a maximum value, reached around 10% pilot fuel energy share. Fluidbed results are not plotted as only two conditions provide stable combustions. It has to be noted that the Updraft composition induces a lower combustion efficiency than Downdraft but a better thermal one. This is despite the fact that CA50 is very similar between the two compositions for the same pilot fuel amount (Figure 8). Due to the higher H2 content, Downdraft has a greater flame speed (Table 1) thus leading to a better consumption of fresh gases. On the other hand, this higher H2 content could lead to higher combustion temperature and therefore more heat losses thus depleting the thermal efficiency as highlighted numerically by Kousheshi et al. [30]. The emissions data show that CO and soot emissions are

negatively affected by the increase in decane quantity, without any bell or inverse bell shape: more diesel type fuel induces more unburnt carbonaceous exhaust gases except THC, i.e. a slight reduction seems to occur with decane addition for the updraft composition. The level of soot was so low than no value could be measured, for fuel amount lower than 12% energy share similarly to what was observed by Papagiannakis et al. [17] with methane/diesel dual-fuel. Yet when reaching 20% for E_{pilot}, soot emissions rise up to significant value of 6-9 g/kWh. It is also clear that NO_x emissions strongly increase as a function of decane amount, due to the increase of in-cylinder temperatures. It is interesting to notice, both CO and NOx are minimum for the same E_{pilot} and rises with E_{pilot} increase. The syngas is globally a low NOx fuels, its combustion temperature is very low compare to other fuels. Moreover since the equivalence ratio stays poor in the whole study the CO and HC are also low. Yet, when increasing decane quantity both NOx and CO rise simultaneously because it will induce a combustion temperature increase leading to higher NOx and an increase of liquid quantity that leads to a poorer mixing and evaporation that leads to higher CO and HC. The effects of CO_2 on NO_x emissions will be discussed further on the final part of this work.

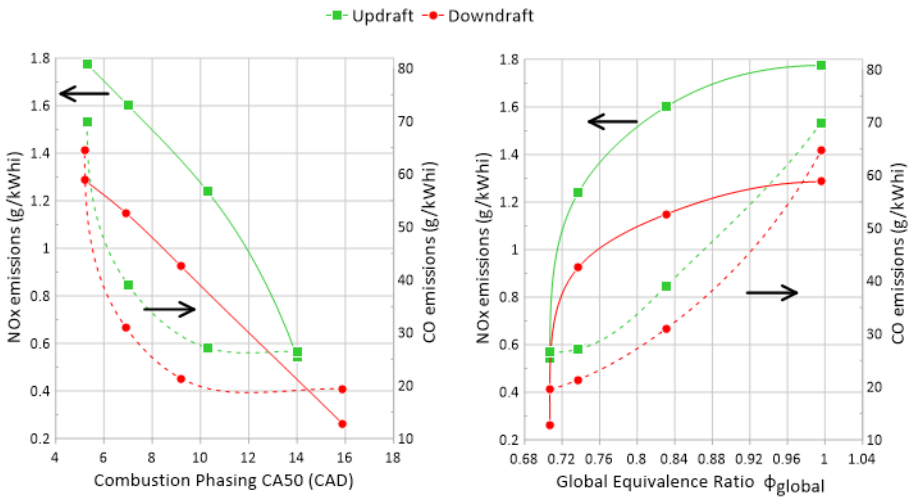

Figure 10: Specific emissions of NO_x (continuous line) and CO (dashed line) as a function of combustion phasing (left) and global equivalence ratio (right) ($\mathbf{1200\ RPM\ P_{intake} = 1\ bar, T_{intake} = 300K, \phi_{premixed} = 0.7}$).

In Figure 10, NO_x and CO emissions are presented as a function of CA50 and ϕ_{global}. Regarding the relationship between emissions and combustion phasing it is clear that, for this premixed equivalence ratio, CO emissions reach a plateau for CA50 > 9 CAD ATDC while NO_x emissions decrease almost linearly with CA50, as the in-cylinder temperature is higher for shorter combustion. The NOx emissions as function of the global equivalence ratio follows the decane share, and seems to reach a plateau when the global equivalence ratio tends to 1. Meanwhile, the increase in CO emissions seems not to reach a plateau as usually in SI engines: CO increases with the global equivalence ratio increase.

3.3 Effect of CH_4 and CO_2 concentration

To give further insight on the roles of CH_4 and CO_2 on performance and emissions, complementary measurements were performed with the composition variations as in Table 5. The variation consists of maintaining H_2 and CO volume fractions constant while adjusting the N_2 volume fraction to compensate CO_2 or CH_4 variations. The variations are designated by the composition (FB, UD, DD for Fluidbed, Updraft, Downdraft respectively), from which the H_2 and CO content is kept, followed by an index that refers to the CO_2 or CH_4 content. The variation FB–20_{CO2} is greyed out as no stable operation could be obtained. The Madison kinetics mechanism[26] was selected in combination with the PREMIX and EQUIL CHEMKIN ANSYS PRO codes to estimate laminar flame speed and flame temperature respectively, by considering initial conditions equal to those in the cylinder at the start of injection (864 K and 30 bar, $\phi = 0.7$). This mechanism was validated for this purpose in a previous study[25]. Premixed equivalence ratio was kept constant at 0.7 and the injection with a duration of 400 μs (i.e. 0.32 mg corresponding to $E_{pilot} \approx 1.65\%$) started at -18 CAD BTDC.

Table 5: Variations on the original Syngas compositions.

Variation	H2 ($\%_{vol}$)	CO ($\%_{vol}$)	CO2 ($\%_{vol}$)	CH4 ($\%_{vol}$)	N2 ($\%_{vol}$)	Adiabatic Equilibrium Flame Temperature (K)	Laminar Flame Speed (cm/s)
FB – $0_{CO2-CH4}$	9	14	0	0	77	1868	32.3
FB – 10_{CO2}			10	0	67	1834	24.3
FB – 20_{CO2}			20	0	57	1802	14.9
FB – 2.5_{CH4}			0	2.5	74.5	1955	33.0
FB – 5_{CH4}			0	5	72	2016	35.0
FB - Reference			20	7	50	2004	26.4
UD – $0_{CO2-CH4}$	11	24	0	0	65	2092	61.5
UD – 10_{CO2}			10	0	55	2059	51.1
UD – 20_{CO2}			20	0	45	2028	41.9
UD – 2.5_{CH4}			0	2.5	62.5	2131	59.5
UD – 5_{CH4}			0	5	60	2160	58.2
UD - Reference			9	3	53	2112	51.1
DD – $0_{CO2-CH4}$	17	21	0	0	62	2120	83.0
DD – 10_{CO2}			10	0	52	2088	69.1
DD – 20_{CO2}			20	0	42	2057	57.9
DD – 2.5_{CH4}			0	2.5	59.5	2154	75.4
DD – 5_{CH4}			0	5	57	2178	71.2
DD – Reference			13	1	48	2095	62.7

In Figure 11, the effect of CO_2 and CH_4 content on HRR is highlighted. CO_2 addition to Syngas delays the onset of combustion and extends the combustion duration. This effect has

been well described by Xiang et al.[31] and Halter et al.[32] for CH_4/CO_2/Air mixtures where the dilution, thermal and chemical contributions of CO_2 to the reduction of laminar flame speed have been quantified. Since the total dilution amount, i.e. N_2 + CO_2 quantity, is kept constant, the effect seen here is both related to the thermal (increased heat capacity of the charge → reduction of charge temperature) and chemical effects. Moreover, the two combustion stages present for downdraft and updraft without any CO_2 (DD – $0_{CO2\text{-}CH4}$ and UD – $0_{CO2\text{-}CH4}$ respectively), are less evident with CO_2 addition. On the other hand, the addition of CH_4 advances the start of combustion and makes it easier to distinguish the two combustion phases. This could indicate that the H_2 in the syngas might be consumed first, contributing to the initial rise in HRR, followed by the slower-burning CO and CH_4.

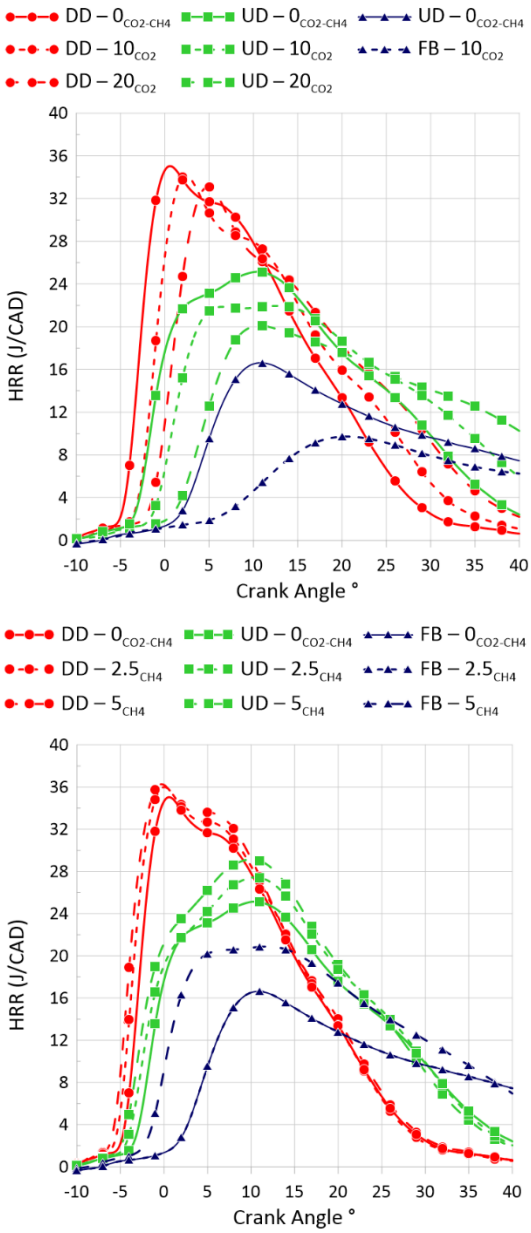

Figure 11: Heat Release Rate profiles for varying CO_2 (top) and CH_4 (bottom) contents ($\mathbf{1200\ RPM}\ P_{intake} = \mathbf{1\ bar},\ T_{intake} = \mathbf{300K},\ \phi_{premixed} = 0.7\ SOI = -18\ CAD\ BTDC$).

The resulting efficiencies and emissions from the variations tested are presented in Figure 12. Soot emissions are not presented because they are always under the detection limit. By replacing N_2 with CO_2, the decrease of combustion efficiency induces CO and THC increase

but a reduction of NO_x emissions, due to the delay of the combustion phasing as the start of injection was maintained constant and not optimized.

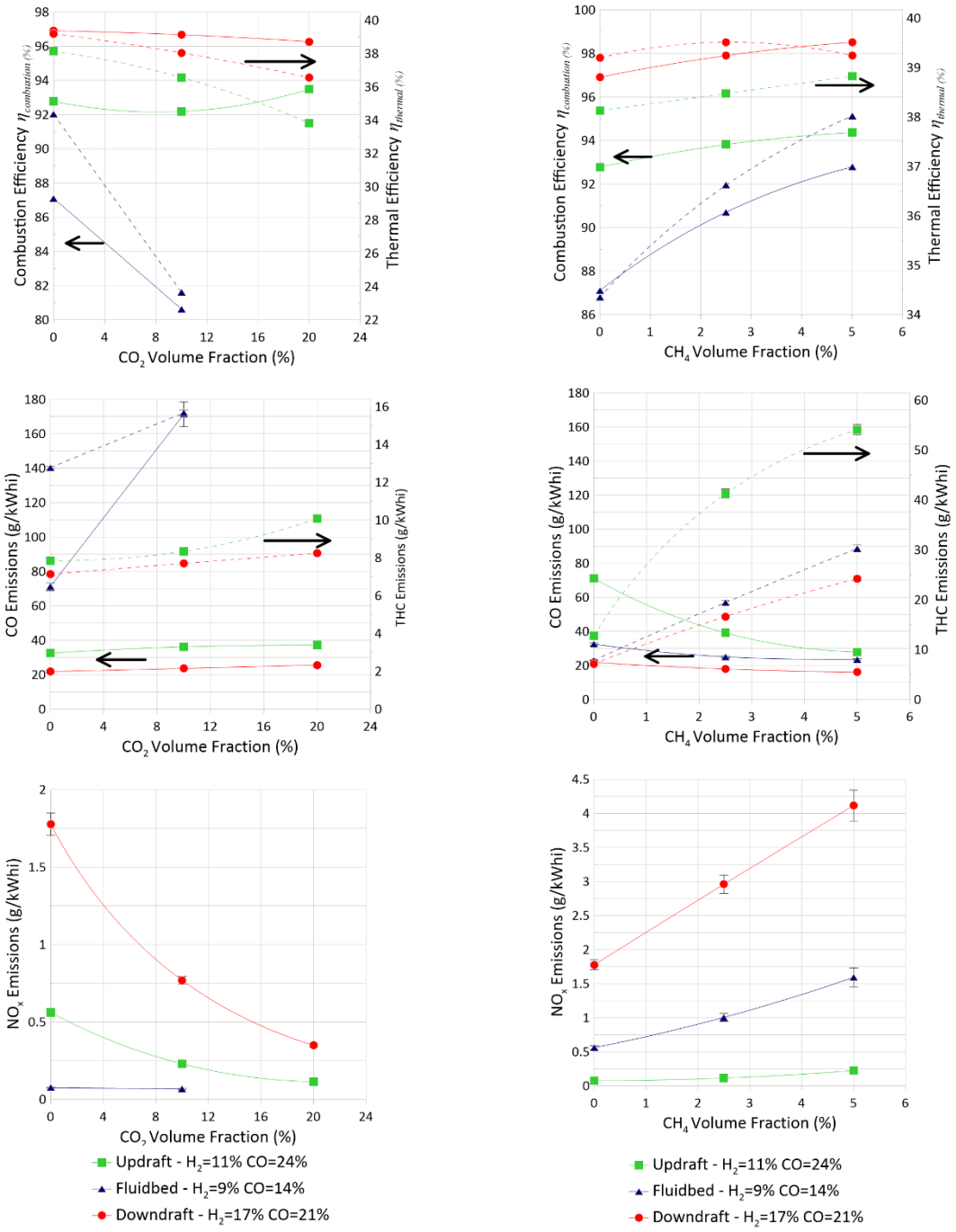

a) Effect of CO2 content b) Effect of CH4 content

Figure 12. Effect of Syngas components a) CO2 and b) CH4 on engine efficiencies and exhaust emissions (1200 RPM, $P_{intake} = 1$ bar, $T_{intake} = 300K$, $\phi_{premixed} = 0.7$, $SOI = -17$ $BTDC$).

Figure 12 b) indicated that CH_4 addition increases both thermal and combustion efficiencies resulting in lower CO emissions. Despite the overall higher combustion efficiencies, THC emissions increase with CH_4 addition due to the increase of unburned CH_4 itself. Even if the amount of CH4 added remains low, the increase of CH4 % induces an increase of NOX emissions, mainly due to higher in-cylinder temperatures, as predicted the higher adiabatic temperature values in Table 5. Due to the higher H_2 content, Downdraft provides a greater combustion development speed thus leading to a better consumption of fresh gases. On the other hand, this higher H_2 content could lead to higher combustion temperature and therefore more heat losses thus depleting the thermal efficiency.

3.4 Relationship between fundamental composition properties and engine operation

In order to predict the effect of syngas composition, it is important to highlight the relationship between the fundamental properties of the composition (such as laminar flame speeds, LFS, or adiabatic flame temperature, T_{ad}) and the resulting engine performance and emissions. For that, empirical correlations are suggested in Figure 13 and 13 to identify the effect of properties variations in Table 5 to the combustion durations and stability and NO_x, THC and CO emissions.

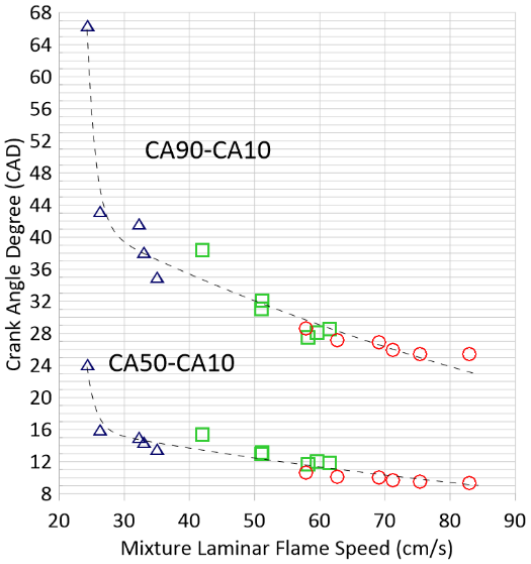

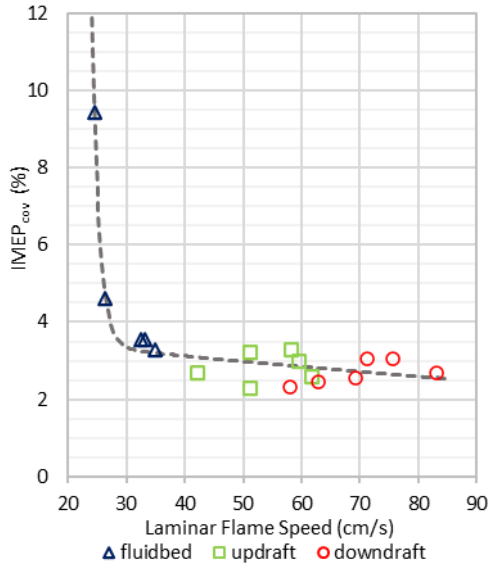

Figure 13: Relationship between combustion duration and stability ($IMEP_{cov}$) as a function of syngas Laminar Flame Speed. (1200 RPM, $P_{intake} = 1$ bar, $T_{intake} = 300$K, $\phi_{premixed} = 0.7$ $SOI = -18$ CAD $BTDC$).

First flame development stage duration (CA50-CA10) and total combustion duration (CA90-CA10) clearly decrease with the laminar flame speed with a clear transition when the flame speed goes under a certain level probably due to the combustion instabilities linked to the low value of LFS in the case of fluidbed. A similar behavior was observed by Lhuillier et al.[33] for NH_3/H_2 mixtures in a SI engine. Nevertheless, while the trend is clear for the whole of the 17 compositions tested, locally, the experimental points seem to group together as a function

of H_2/CO contents. In Figure 13b, one can note that when the composition of a syngas/air mixture induces a laminar flame speed lower than 40 cm/s, as it is for fluidbed composition, $IMEP_{cov}$ rises sharply. Yet, for LFS $> 40\ cm/s$, the stability is not affected by any laminar flame speed change.

In Figure 14a, total hydrocarbon (THC) emissions increase with the addition of CH_4, as the number of HC increase, indicating that the part of intermediate CH due to the decane oxidation (or to crevice trapping) is lower. In the case of CO emissions (Figure 14.b), same linear dependency can be noted of Downdraft and Updraft compositions but the exhaust CO values are less than 10 times the CO quantity introduced, due to the oxidation of the CO during the combustion process. Yet, the high $IMEP_{cov}$ for Fluidbed induces higher combustion instabilities leading to high CO emissions even if the CO flowrate at the intake is lower.

As the main source of NOx for these fuels is due to the thermal mechanism, NO_x production rate increases exponentially with the adiabatic flame temperatures as shown in Figure 14.c. The increase of H_2 contents as in Downdraft induces higher NOx emissions: exponential evolution as a function of adiabatic temperature is accurate but with different coefficients, dependent to the syngas compositions. Notably, for very similar adiabatic flame temperatures, the Downdraft compositions produce more NO_x than the Updraft compositions. Last, as highlighted by Rakopoulos et al. [34], the oxygen content has a significant effect on performances and emissions. When comparing updraft and fluidbed, they exhibit very similar H2 content but CO and therefore oxygen content is much higher for updraft. Rakopoulos et al. showed that NO emissions increase with the degree of oxygenation which could explain the higher NOx levels for updraft mixtures compared to fluidbed.

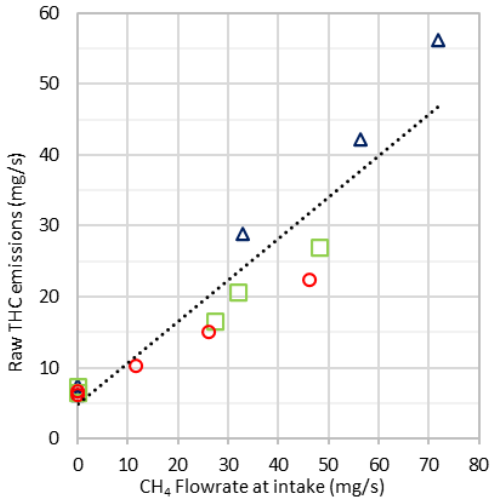

441

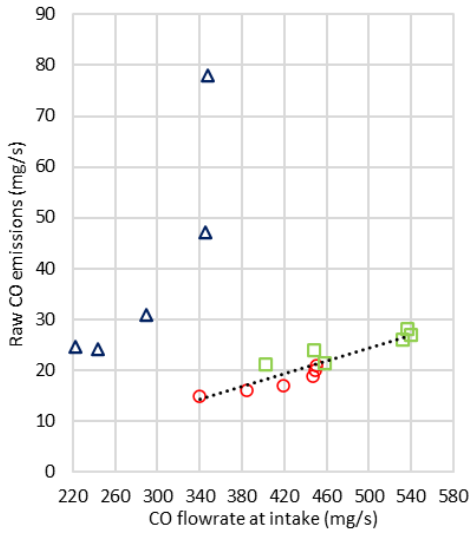

442

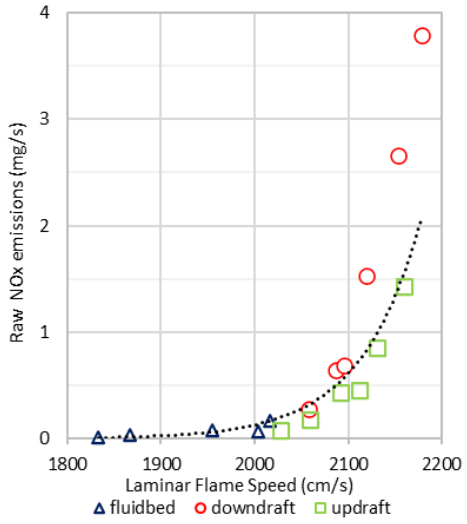

443

444 **Figure 14: Relationship between THC emissions and intake CH4 (a), Exhaust and**

445 **Intake CO (b), NOx and T_{ad} (c).**

$$(\mathbf{1200\ RPM\ P_{intake} = 1\ bar\ T_{intake} = 300\ K}, \boldsymbol{\phi_{premixed} = 0.7\ SOI = -18\ CAD\ BTDC}).$$

4 Conclusion

In this study, the effects of the syngas composition on engine operation parameters and emissions are presented and discussed as a function of the syngas/air equivalence ratio in the intake charge and the more reactive fuel pilot injected mass. The main conclusions from these results are the followings:

- With minimal tuning and no engine geometry optimization, indicated thermal efficiencies of over 38% were obtained with all compositions with syngas representing almost 90% of the total energy supplied to the engine.
- Heat release rate profiles showed a strong influence of syngas H_2 content on combustion duration and phasing.
- CO_2, present on most of syngas compositions, plays an important role in reducing NO_x emissions in dual-fuel operating mode. While this can be interesting for complying with emission regulations, too much CO_2 on Syngas can lead to poor combustion efficiency requiring more reactive fuel in the pilot injection in order to ensure stable engine operation but increase of soot emissions is the consequence.
- The development of the in-cylinder combustion can be empirically predicted based only on known fundamental properties of the syngas composition as the laminar flame speed. The emissions also can be predicted as a function of the different components in the syngas. This could be useful for live tuning of the engine's control strategy to as a function of the composition fluctuations of the gasifier product gas. Accurate predictions would require a better knowledge of secondary chemical and physical effects of varying syngas compositions such as stretch sensitivity or chemical pathways and species rate of production.

Finally, further studies on optical engine would be necessary to give a better understanding on different combustion steps (as diffusion phase, premixed or cool flame due to pre-ignition) and flame propagation as it relates to the different compositions and their respective fundamental combustion properties.

5 Acknowledgement

The research leading to these results has received funding from the French Government's "Investissement d'Avenir" program: "Laboratoire d'Excellence CAPRYSSES" (Grant No ANR-11-LABX-0006–01) and Région Centre-Val de Loire.

6 References

[1] IEA, Net Zero by 2050: A Roadmap for the Global Energy Sector, 2021. www.iea.org/t&c/ (accessed November 3, 2021).

[2] H. Wu, M.A. Hanna, D.D. Jones, Life cycle assessment of greenhouse gas emissions of feedlot manure management practices: Land application versus gasification, Biomass and Bioenergy. 54 (2013) 260–266. https://doi.org/10.1016/J.BIOMBIOE.2013.04.011.

[3] F. Ardolino, U. Arena, Biowaste-to-Biomethane: An LCA study on biogas and syngas roads, Waste Manag. 87 (2019) 441–453. https://doi.org/10.1016/j.wasman.2019.02.030.

[4] D. Schweitzer, A. Gredinger, M. Schmid, G. Waizmann, M. Beirow, R. Spörl, G. Scheffknecht, Steam gasification of wood pellets, sewage sludge and manure: Gasification performance and concentration of impurities, Biomass and Bioenergy. 111 (2018) 308–319. https://doi.org/https://doi.org/10.1016/j.biombioe.2017.02.002.

[5] A.V. Bridgwater, The technical and economic feasibility of biomass gasification for power generation, Fuel. 74 (1995) 631–653. https://doi.org/10.1016/0016-2361(95)00001-L.

[6] R. Thomson, P. Kwong, E. Ahmad, K.D.P. Nigam, Clean syngas from small commercial biomass gasifiers; a review of gasifier development, recent advances and performance evaluation, Int. J. Hydrogen Energy. 45 (2020) 21087–21111. https://doi.org/10.1016/j.ijhydene.2020.05.160.

[7] G. Sridhar, P.J. Paul, H.S. Mukunda, Biomass derived producer gas as a reciprocating engine fuel - An experimental analysis, Biomass and Bioenergy. 21 (2001) 61–72. https://doi.org/10.1016/S0961-9534(01)00014-9.

[8] A. Arunachalam, D.B. Olsen, Experimental evaluation of knock characteristics of producer gas, Biomass and Bioenergy. 37 (2012) 169–176. https://doi.org/10.1016/j.biombioe.2011.12.016.

[9] H. Guo, W.S. Neill, B. Liko, The combustion and emissions performance of a syngas-diesel dual fuel compression ignition engine, ASME 2016 Intern. Combust. Engine Fall Tech. Conf. ICEF 2016. (2016). https://doi.org/10.1115/ICEF20169367.

[10] C.A. Rinaldini, G. Allesina, S. Pedrazzi, E. Mattarelli, T. Savioli, N. Morselli, M. Puglia, P. Tartarini, Experimental investigation on a Common Rail Diesel engine partially fuelled by syngas, Energy Convers. Manag. 138 (2017) 526–537. https://doi.org/10.1016/j.enconman.2017.02.034.

[11] B.B. Sahoo, N. Sahoo, U.K. Saha, Effect of engine parameters and type of gaseous fuel on the performance of dual-fuel gas diesel engines-A critical review, Renew. Sustain. Energy Rev. 13 (2009) 1151–1184. https://doi.org/10.1016/j.rser.2008.08.003.

[12] M. Costa, M. La Villetta, N. Massarotti, D. Piazzullo, V. Rocco, Numerical analysis of a compression ignition engine powered in the dual-fuel mode with syngas and biodiesel, Energy. 137 (2017) 969–979. https://doi.org/https://doi.org/10.1016/j.energy.2017.02.160.

[13] Z. Xu, M. Jia, Y. Li, Y. Chang, G. Xu, L. Xu, X. Lu, Computational optimization of

fuel supply, syngas composition, and intake conditions for a syngas/diesel RCCI engine, Fuel. 234 (2018) 120–134. https://doi.org/https://doi.org/10.1016/j.fuel.2018.07.003.

[14] N. Stylianidis, U. Azimov, A. Maheri, E. Tomita, N. Kawahara, Chemical kinetics and CFD analysis of supercharged micro-pilot ignited dual-fuel engine combustion of syngas, Fuel. 203 (2017) 591–606. https://doi.org/https://doi.org/10.1016/j.fuel.2017.04.125.

[15] M. Sharma, R. Kaushal, Performance and exhaust emission analysis of a variable compression ratio (VCR) dual fuel CI engine fuelled with producer gas generated from pistachio shells, Fuel. 283 (2021) 118924. https://doi.org/10.1016/j.fuel.2020.118924.

[16] M. Mohon Roy, E. Tomita, N. Kawahara, Y. Harada, A. Sakane, Performance and emission comparison of a supercharged dual-fuel engine fueled by producer gases with varying hydrogen content, Int. J. Hydrogen Energy. 34 (2009) 7811–7822. https://doi.org/10.1016/j.ijhydene.2009.07.056.

[17] R.G. Papagiannakis, S.R. Krishnan, D.C. Rakopoulos, K.K. Srinivasan, C.D. Rakopoulos, A combined experimental and theoretical study of diesel fuel injection timing and gaseous fuel/diesel mass ratio effects on the performance and emissions of natural gas-diesel HDDI engine operating at various loads, Fuel. 202 (2017) 675–687. https://doi.org/10.1016/J.FUEL.2017.05.012.

[18] A. Srna, B. von Rotz, K. Herrmann, K. Boulouchos, G. Bruneaux, Experimental investigation of pilot-fuel combustion in dual-fuel engines, Part 1: Thermodynamic analysis of combustion phenomena, Fuel. (2019) 115642. https://doi.org/10.1016/J.FUEL.2019.115642.

[19] A. Srna, B. von Rotz, M. Bolla, Y.M. Wright, K. Herrmann, K. Boulouchos, G. Bruneaux, Experimental investigation of pilot-fuel combustion in dual-fuel engines,

546 Part 2: Understanding the underlying mechanisms by means of optical diagnostics,
547 Fuel. (2019) 115766. https://doi.org/10.1016/J.FUEL.2019.115766.
548 [20] A. Srna, M. Bolla, Y.M. Wright, K. Herrmann, R. Bombach, S.S. Pandurangi, K.
549 Boulouchos, G. Bruneaux, Effect of methane on pilot-fuel auto-ignition in dual-fuel
550 engines, Proc. Combust. Inst. 37 (2019) 4741–4749.
551 https://doi.org/10.1016/J.PROCI.2018.06.177.
552 [21] L. Wei, P. Geng, A review on natural gas/diesel dual fuel combustion, emissions and
553 performance, Fuel Process. Technol. 142 (2016) 264–278.
554 https://doi.org/10.1016/J.FUPROC.2015.09.018.
555 [22] V. Pessina, A. D'Adamo, C. Iacovano, S. Fontanesi, S. Martinez, P. Lacava, Numerical
556 Simulation of Syngas Blends Combustion in a Research Single-Cylinder Engine, SAE
557 Tech. Pap. 2019 (2019) 1–14. https://doi.org/10.4271/2019-24-0094.Abstract.
558 [23] E. Monteiro, M. Bellenoue, J. Sotton, N.A. Moreira, S. Malheiro, Laminar burning
559 velocities and Markstein numbers of syngas-air mixtures, Fuel. 89 (2010) 1985–1991.
560 https://doi.org/10.1016/j.fuel.2009.11.008.
561 [24] E. Monteiro, A. Rouboa, Measurements of the laminar burning velocities for typical
562 syngas-air mixtures at elevated pressures, J. Energy Resour. Technol. Trans. ASME.
563 133 (2011). https://doi.org/10.1115/1.4004607.
564 [25] R. Rabello de Castro, P. Brequigny, J.P. Dufitumukiza, C. Mounaïm-Rousselle,
565 Laminar flame speed of different syngas compositions for varying thermodynamic
566 conditions, Fuel. 301 (2021) 121025. https://doi.org/10.1016/j.fuel.2021.121025.
567 [26] S. Ren, S.L. Kokjohn, Z. Wang, H. Liu, B. Wang, J. Wang, A multi-component wide
568 distillation fuel (covering gasoline, jet fuel and diesel fuel) mechanism for combustion
569 and PAH prediction, Fuel. 208 (2017) 447–468.
570 https://doi.org/10.1016/j.fuel.2017.07.009.

571 [27] G. Woschni, A universally applicable equation for the instantaneous heat transfer
572 coefficient in the internal combustion engine, SAE Tech. Pap. (1967).
573 [28] A.E. Dhole, R.B. Yarasu, D.B. Lata, Effect of hydrogen and producer gas as secondary
574 fuels on combustion parameters of a dual fuel diesel engine, Appl. Therm. Eng. 108
575 (2016). https://doi.org/10.1016/j.applthermaleng.2016.07.157.
576 [29] E.G. Giakoumis, D.C. Rakopoulos, C.D. Rakopoulos, Combustion noise radiation
577 during dynamic diesel engine operation including effects of various biofuel blends: A
578 review, Renew. Sustain. Energy Rev. 54 (2016) 1099–1113.
579 https://doi.org/10.1016/J.RSER.2015.10.129.
580 [30] N. Kousheshi, M. Yari, A. Paykani, A. Saberi Mehr, G.F. de la Fuente, Effect of
581 Syngas Composition on the Combustion and Emissions Characteristics of a
582 Syngas/Diesel RCCI Engine, Energies. 13 (2020) 212.
583 https://doi.org/10.3390/en13010212.
584 [31] L. Xiang, H. Chu, F. Ren, M. Gu, Numerical analysis of the effect of CO2 on
585 combustion characteristics of laminar premixed methane/air flames, J. Energy Inst. 92
586 (2019) 1487–1501. https://doi.org/10.1016/j.joei.2018.06.018.
587 [32] F. Halter, F. Foucher, L. Landry, C. Mounaim-Rousselle, Effect of dilution by nitrogen
588 and/or carbon dioxide on methane and iso-octane air flames, Combust. Sci. Technol.
589 181 (2009) 813–827. https://doi.org/10.1080/00102200902864662.
590 [33] C. Lhuillier, P. Brequigny, F. Contino, C. Mounaïm-Rousselle, Experimental study on
591 ammonia/hydrogen/air combustion in spark ignition engine conditions, Fuel. 269
592 (2020) 117448. https://doi.org/10.1016/j.fuel.2020.117448.
593 [34] D.C. Rakopoulos, C.D. Rakopoulos, E.G. Giakoumis, R.G. Papagiannakis, Evaluating
594 Oxygenated Fuel's Influence on Combustion and Emissions in Diesel Engines Using a
595 Two-Zone Combustion Model, J. Energy Eng. 144 (2018) 04018046.

https://doi.org/10.1061/(ASCE)EY.1943-7897.0000556.